Applied Catalysis B: Environmental 257 (2019) 117934

Contents lists available at ScienceDirect

Applied Catalysis B: Environmental

journal homepage: www.elsevier.com/locate/apcatb

Noble metal free CdS@CuS-Ni$_x$P hybrid with modulated charge transfer for enhanced photocatalytic performance

Yue-Hua Li[a,b], Ming-Yu Qi[a,b], Jing-Yu Li[a,b], Zi-Rong Tang[b], Yi-Jun Xu[a,b,*]

[a] State Key Laboratory of Photocatalysis on Energy and Environment, College of Chemistry, Fuzhou University, Fuzhou, 350116, PR China
[b] College of Chemistry, New Campus, Fuzhou University, Fuzhou, 350116, PR China

ARTICLE INFO

Keywords:
Noble metal free
Transition metal phosphides
1D CdS
Charge transfer

ABSTRACT

Constructing low-cost and highly active photocatalysts is extremely desirable for converting solar energy into chemical fuels. Herein, we report a one-dimensional (1D) CdS@CuS-Ni$_x$P (CCN) core-shell heterostructure catalyst for effective photocatalytic hydrogen (H_2) evolution with modulated charge transfer, which exhibits remarkably higher activity than bare CdS nanowires (NWs). The evenly distributed and closely contacted CdS@CuS (CC) heteroepitaxial nanomaterial constructs a type-I heterostructure for improved photoinduced charge carrier separation. The Ni$_x$P nanoparticles (NPs), which act as a cocatalyst, not only contribute to constructing three-level charge transfer by capturing the photogenerated electrons, but also provide active sites for proton reduction. In addition, the cocatalyst strategy reported here can be extended to other transition metal phosphide (TMP). Mechanistic studies suggest that the cooperative synergy of three-level charge transfer and introduction of reaction sites results in a significant enhancement of photoactivity for H_2 evolution.

1. Introduction

Harvesting solar energy to drive photocatalytic production of hydrogen (H_2) is an ideal strategy to meet the increasing global energy demand [1,2]. Among all the semiconductor photocatalysts, cadmium sulfide (CdS) is one of the most promising materials for photocatalytic H_2 production owing to its desirable band gap and suitable conduction band edge positions [2]. However, insufficient photoinduced charge carrier separation and undesirable photocorrosion result in low solar-to-H_2 conversion efficiency of CdS [3]. In order to overcome these obstacles, constructing CdS-based heterostructure systems has been employed to ameliorate charge separation and transfer dynamics [4].

Copper sulfide (CuS), which possesses excellent optical, electrical and catalytic properties, has great potential to form CdS@CuS (CC) heteroepitaxial nanomaterial with low lattice mismatch and good matchable band gap for efficient charge separation and transfer [5,6]. However, considering the large exciton binding energy of CdS, maximizing the charge carrier separation efficiency by only one charge separation channel is difficult to achieve [5]. In this regard, introducing appropriate cocatalysts to form semiconductor-based heterostructure is an effective strategy to optimize the performance of photocatalyst by trapping the charge carriers, suppressing the recombination of photogenerated electron-hole pairs or providing active sites for target redox reaction [7]. In recent years, much theoretical and experimental effort has been devoted to demonstrating that the transition metal phosphides (TMPs) formed by alloying metals and phosphorus, such as FeP [8,9], CoP [10,11], Ni_2P [12,13], Cu_3P [14,15], and WP [16], are suitable for enhancing the activity of water splitting [17]. Among them, the nickel phosphide (Ni$_x$P), which can extract electrons from semiconductor and lower the H^+ reduction overpotential, is a noble-metal-free, low-cost, non-toxicity and highly efficient cocatalyst for photocatalytic H_2 production [18–21]. In addition, density functional theory (DFT) calculations elucidate that the Ni hollow site and Ni-P bridge site in Ni$_x$P exhibit a propitious ensemble effect to promote H_2 generation [22].

Herein, we have developed a two-step route of using cation exchange and the photochemical reduction method to synthesize ternary CdS@CuS-Ni$_x$P (CCN) core-shell heterostructure composite catalyst for modulating charge separation and thus improving the activity of photocatalytic H_2 evolution. In this ternary heterostructure, the CuS is uniformly decorated on the one dimensional (1D) CdS NWs by cation exchange method, thereby constructing a tightly connected type-I heterostructure for assisting the separation of photoinduced electron-hole pairs [3]. The Ni$_x$P nanoparticles (NPs) photodeposited onto the CC NWs play the dual roles in trapping the photogenerated electrons and providing active sites for proton reduction to produce H_2 [23]. Consequently, the three-level charge transfer over CCN composite is

* Corresponding author at: State Key Laboratory of Photocatalysis on Energy and Environment, College of Chemistry, Fuzhou University, Fuzhou, 350116, PR China.
E-mail address: yjxu@fzu.edu.cn (Y.-J. Xu).

https://doi.org/10.1016/j.apcatb.2019.117934
Received 16 April 2019; Received in revised form 12 June 2019; Accepted 6 July 2019
Available online 08 July 2019

comprised of the matched energy level position between CdS and CuS, and the capture of photogenerated electrons by Ni_xP NPs. As such, the optimal CCN photocatalytic system exhibits 29 and 5 fold enhancement on photocatalytic H_2 production compared with bare CdS NWs and CC-Pt composite, respectively. The joint analysis of photoelectrochemical characterizations, steady-state photoluminescence (PL) and time-resolved photoluminescence (TRPL) spectra demonstrates that the synergistic effect of three-level charge transfer and the addition of active sites lead to the boosted photocatalytic performance.

2. Experimental section

2.1. Materials

Nickel (II) chloride hexahydrate ($NiCl_2{\cdot}6H_2O$), cadmium chloride ($CdCl_2{\cdot}2.5H_2O$), cupric nitrate ($Cu(NO_3)_2$), sodium diethyldithiocarbamate trihydrate ($C_5H_{10}NNaS_2{\cdot}3H_2O$), ethylenediamine ($C_2H_8N_2$), cobalt (II) chloride hexahydrate ($CoCl_2{\cdot}6H_2O$), absolute ethanol (C_2H_5OH), sodium hypophosphite (NaH_2PO_2), were supplied by Sinopharm Chemical Reagent Co., Ltd. (Shanghai, China). All materials were used as received without further treatment. Deionized (DI) water used in the experimental procedure was obtained from local sources.

2.2. Synthesis

2.2.1. Preparation of CdS nanowires (NWs)

We used a solvothermal method to synthesize CdS NWs [24,25]. As generalized in Fig. S**1**, 30 mL of $C_5H_{10}NNaS_2$ solution was injected into the $CdCl_2$ solution under magnetic stirring to obtained the cadmium diethyldithiocarbamate ($Cd(S_2CNEt_2)_2$). The obtained white precipitate was dried in an electronic oven at 353 K. The autoclave was kept at 453 K for 24 h after 2.248 g of ($Cd(S_2CNEt_2)_2$) and 80 mL of ethylenediamine were added into the Teflon-lined stainless steel autoclave with a volume of 100 mL. The resultant yellowish sediment was rinsed with DI water and ethanol to remove the residual organic solvents and then dried at 343 K for 12 h.

2.2.2. Preparation of CdS@CuS (CC) NWs

CC NWs were prepared by a cation exchange method according to the previously reported literature [26]. Typically, CdS NWs (0.1 g) were first dispersed into DI water by sonication for 10 min, followed by addition of a calculated amount of $Cu(NO_3)_2$ aqueous solution (1 mM). After 60 min of stir, the samples were separated by filtration and rinsed with DI water. The final products were dried in oven at 333 K. The theoretical molar ratios of CuS were 0.5, 1 and 3 mol% and the samples were labeled as CC-0.5, CC-1, CC-3, respectively. As revealed below, the CC-1 sample displays the highest hydrogen (H_2) production activity among the CC NWs composites, and thus CC-1 NWs composite is selected to investigate the effects of Ni_xP.

2.2.3. Preparation of CdS@CuS-Ni_xP (CCN) NWs

CCN NWs were prepared by a modified *in situ* photochemical deposition strategy [27]. Typically, 40 mg of the prepared CC-1 NWs were first dispersed in a 40 mL mixture of DI water (32 mL) and ethanol (8 mL) by sufficient sonication, followed by addition of a calculated amount of $NiCl_2$ and NaH_2PO_2. After using nitrogen (N_2) bubbling (flow rate = 50 mL min^{-1}) for 30 min to eliminate air from the mixture, the yellow suspension was illuminated under visible light ($\lambda > 420$ nm) for 40 min with continuous N_2 bubbling. The final products were collected by filtration and rinsed with DI water. Finally, the products were dried by a gentle stream of N_2 at room temperature. The obtained CCN NWs with different weight ratios of Ni_xP (0.5%, 1%, 1.5%, 2%) were labeled as CCN-0.5, CCN-1, CCN-1.5, CCN-2, respectively. Notably, the samples should be preserved in the N_2 atmosphere.

2.2.4. Preparation of CdS-Ni_xP (CN)

The preparation method of CN NWs was the same as that of CCN NWs except using CdS NWs to replace CC-1 NWs. The samples with different weight ratios of Ni_xP were denoted as CN-0.5, CN-1, CN-1.5, CN-3, CN-5, respectively.

2.2.5. Preparation of CdS@CuS-Co_xP (CC-Co_xP)

The preparation method of CC-Co_xP NWs was the same as that of CCN NWs except using the $CoCl_2{\cdot}6H_2O$ to replace the $NiCl_2{\cdot}6H_2O$ as the precursor. The samples with different weight ratios of Co_xP were denoted as CC-Co_xP-0.5, CC-Co_xP-1, CC-Co_xP-2, CC-Co_xP-3, respectively.

2.2.6. Preparation of CdS-Pt NWs and CC-Pt-1 NWs

For comparison, the CdS-Pt NWs were synthesized *via* an *in situ* photochemical deposition method. The synthesis process was the same as that of CN NWs except using the H_2PtCl_6 to replace the $NiCl_2{\cdot}6H_2O$ as the precursor. Similarly, the obtained CdS-Pt samples with different weight ratios of Pt were named as CdS-Pt-0.5, CdS-Pt-1, CdS-Pt-2, respectively. The preparation method of CC-Pt-1 NWs (weight ratios of Pt is 1%) was the same as that of CdS-Pt-1 NWs except using CC NWs to replace CdS NWs.

3. Results and discussion

The synthetic process for ternary CdS@CuS-Ni_xP (CCN) core-shell nanowires (NWs) heterostructure is illustrated in Fig. 1**A**. Using the as-prepared CdS NWs as matrix materials, binary CdS@CuS (CC) NWs have been prepared by using copper cations to replace cadmium element on the surface of bare CdS NWs [28]. During cation exchange process, the cations are exchanged within a relatively rigid anion host lattice because of the different diffusivity between anions and cations [29,30]. This method has previously been used to modify the composition of the initial template, while preserving its morphology [29,30]. Subsequently, the Ni_xP nanoparticles (NPs) have been deposited on the CC NWs through a photochemical reduction method [4,27].

The morphology of different samples has been observed by field-emission scanning electron microscopy (FESEM). Fig. 1**B** shows that the 1D CdS NWs with an average diameter of about 50 nm show a relative smooth surface. After cation exchange procedure, as revealed in Fig. 1**C**, the CC NWs still remain their 1D nanostructure but the surface of CC NWs becomes rather rough along the entire length, which should be ascribed to the uniformly dispersed CuS. The Ni_xP NPs deposited on CC NWs are hardly discerned in the SEM images of CCN NWs (Fig. 1**D**) due to their small size and relatively low amounts. Transmission electron microscopy (TEM) measurements have been employed to further characterize the morphology and microstructure of CC and CCN NWs heterostructures. Fig. 1**E** shows that 1D CCN NWs exhibit a clearly defined core-shell structure in which CdS is covered by the CuS. The intimate interfacial contact between CdS and CuS in such core-shell structures is propitious to form junctions between the two components, which is able to improve the separation efficiency of photogenerated charge carriers and thereby boost the photocatalytic activity [2,31]. The Ni_xP NPs with an average size of about 40 nm are tightly photodeposited on the surface of CC NWs. The high-resolution TEM (HRTEM) image of CC NWs shows only one lattice fringe with d-spacing of 0.335 nm, which correspond to the (002) facet of hexagonal CdS (**Fig. S2D**) [3,23]. This result suggests that the crystal lattice of CdS remains unchanged during cation exchange process [3]. As shown in Fig. 1**F**, there is no lattice fringe observed from the deposited Ni_xP NPs, which indicates the amorphous structure of obtained Ni_xP NPs [27]. As disclosed in **Fig. S2E**, all elements in CCN NWs can be detected from energy-dispersive X-ray (EDX) spectroscopy and no other elements can be detected except Mo element from the Mo grid substrate. To further determine the elements distribution, the EDX elemental mapping analysis has been employed. It can be seen from Fig. 1**G** that the Cd and S elements are the main contents of CCN NWs and Cu element is mainly

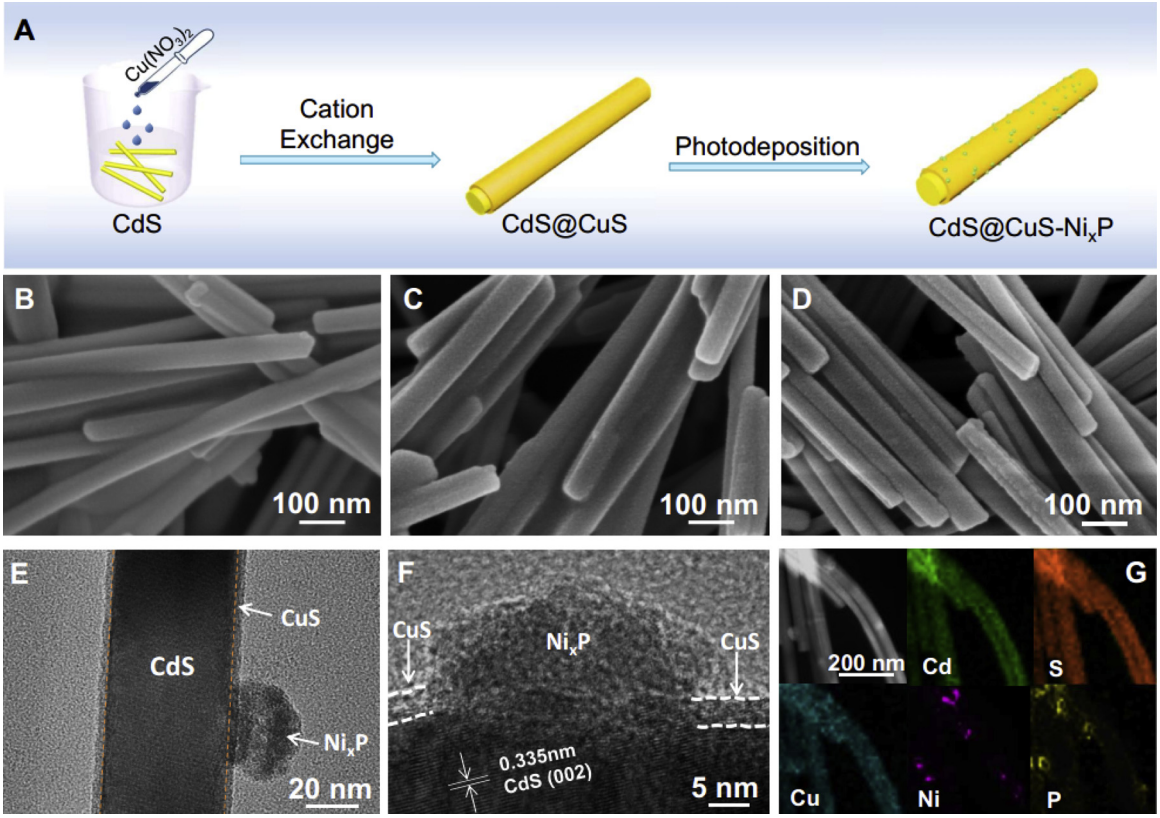

Fig. 1. Schematic illustration of the synthesis of the CCN core-shell NWs (A). FESEM images of CdS NWs (B), CC NWs (C) and CCN NWs (D). TEM image (E), HRTEM image (F) and elemental mapping results (G) of CCN NWs.

distributed around the outside of the CdS NWs, further confirming that Cd element on the surface of CdS NWs is replaced by copper cations [3]. The Ni and P elements are well distributed on the outside surface of CC NWs. These characterization results together prove the successful introduction of CuS and Ni_xP NPs onto the 1D CdS NWs, thereby forming the ternary CCN NWs composite.

The elemental compositions and chemical states of CCN NWs composite can be reflected by X-ray photoelectron spectroscopy (XPS) analysis. Survey spectrum of CCN NWs (Fig. 2**A**) confirms the existence of Cd, S, Cu, Ni and P elements in the ternary sample, which is consistent with the EDX analysis as discussed above. The appearance of C and O elements should be ascribed to the CO_2, H_2O and O_2, which are adsorbed on the surface of CCN NWs [28]. As shown in Fig. 2**B**, the binding energy of Cd $3d_{5/2}$ at 405.2 and Cd $3d_{3/2}$ at 411.9 eV is assigned to Cd^{2+} in CdS [32]. The peaks at 161.5 and 162.7 eV in Fig. 2**C** are characteristic of the S^{2-} in CdS [33]. As seen from Fig. 2D, the double peaks located at 932.7 and 952.5 eV in Cu 2p XPS spectrum are ascribed to the $2p_{3/2}$ and $2p_{1/2}$ of Cu^{2+} in CuS [28]. After 30 s of Ar ion etching, the spectrum of Ni 2p in Fig. 2**E** exhibits two main peaks at 852.8 (Ni $2p_{3/2}$) and 870.2 eV (Ni $2p_{1/2}$), which correspond to Ni species in Ni_xP. Two satellite peaks at 857.2 and 874.6 eV are in agreement with oxidized Ni species arising from superficial oxidation of Ni_xP upon air contact [34]. As shown in Fig. 2**F**, the binding energy at 129.1 eV is attributed to the P (δ^-) of Ni_xP and 133.55 eV is assigned to the phosphate species formed by surface oxidation [17]. It can be concluded from XPS results that the ternary CCN composite has been successfully prepared. The crystalline phase of samples has been detected by X-ray diffraction (XRD). Fig. 2**G** shows that the main diffraction peaks of bare CdS NWs are observed at 2 θ values of 24.80°, 26.50°, 28.20°, 36.70°, 43.70°, 47.90°, 51.90°, and 66.90°, which can be indexed to the (100), (002), (101), (102), (110), (103), (112), and (203) crystal planes of hexagonal CdS (PDF#77-2306), respectively [3]. There are no typical diffraction peaks of CuS and Ni_xP in XRD patterns of binary and ternary samples, revealing that cation exchange method presumably cannot change the crystal lattice structure of pristine CdS and Ni_xP NPs exhibit an amorphous feature [3,27]. These results are in line with those observed in HRTEM images. UV–vis diffuse reflectance spectra (DRS) have been conducted to investigate the optical absorption properties of as-prepared samples. Fig. 2**H** shows that CdS NWs have a distinct absorption edge at wavelength around 520 nm, corresponding to the intrinsic band gap absorption [2]. After loading with CuS and Ni_xP, the optical absorption edge of the CC and CCN NWs resemble that of blank CdS NWs. However, the introduction of different ratios of CuS and Ni_xP has a significant effect on the light absorption properties for the CC and CCN NWs. Namely, with the increase of CuS molar content, there is a gradually enhanced absorbance in the visible light region. After hybridization of Ni_xP with CC NWs, the light absorption of CCN NWs in the same region is continuously enhanced with the increase of Ni_xP weight content, as shown from Fig. 2**I**.

Photocatalytic H_2 evolution performance of as-prepared catalysts has been assessed under visible light irradiation ($\lambda > 420$ nm). As depicted in **Fig. S3A**, blank CdS NWs exhibit H_2 evolution rate of only 0.6 mmol g^{-1} h^{-1}, corresponding to an AQE of 0.38% at 420 nm. This relatively low photoactivity may be ascribed to fast recombination of photogenerated electron-hole pairs and the shortage of active sites for H_2 evolution [7]. After using copper to replace cadmium to form binary composite, CC NWs exhibit elevated H_2 evolution rate and 1% is the optimal loading proportion of CuS (3.23 mmol g^{-1} h^{-1}). The AQE value of the optimal CC-1 NWs at 420 nm is calculated to be 2.12%. The introduction of Ni_xP NPs onto CC-1 NWs contributes to the remarkably improved photoactivity. When loading amount of Ni_xP is 1.5 wt.%, this sample exhibits the optimal photoactivity with the H_2 production rate of 18.16 mmol g^{-1} h^{-1}, equaling to 30 times as high as that of blank CdS NWs (0.6 mmol g^{-1} h^{-1}). The AQE value of CCN-1.5 NWs at 420 nm is calculated to be 13.06%. In addition, binary CN NWs have been prepared, which show obviously lower photoactivity (8.09 mmol

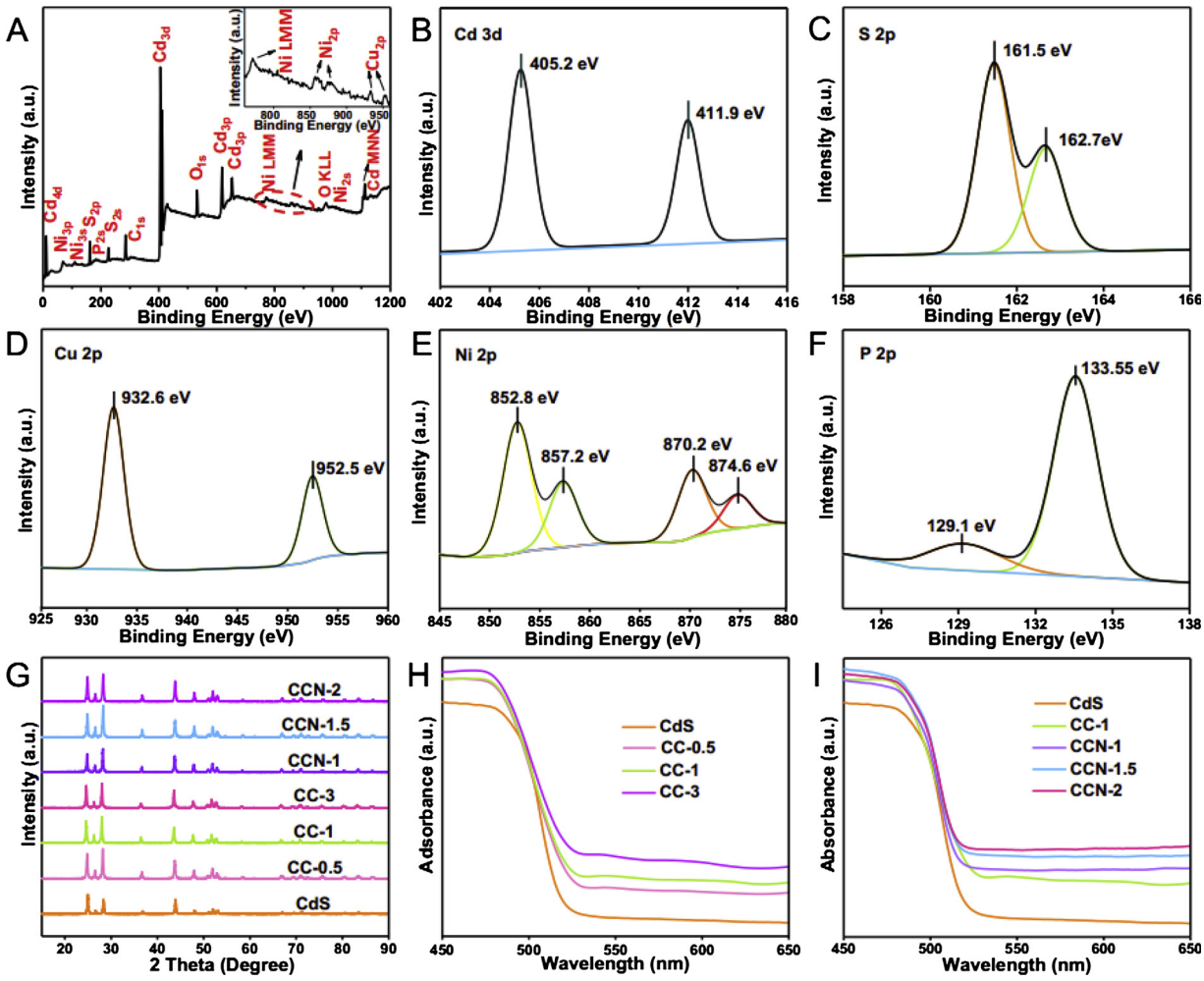

Fig. 2. XPS survey spectrum of CCN NWs (A). For better clarity, the local regions of the XPS survey spectrum depicted by the red oval in (A) is enlarged as the inset of (A). High-resolution XPS spectra of Cd 3d (B), S 2p (C), Cu 2p (D), Ni 2p (E) and P 2p (F) of CCN NWs after 30 s of Ar ion etching. XRD patterns of CdS NWs, CC NWs with different molar ratios of CuS and CCN NWs with different weight ratios of Ni_xP (G). UV–vis diffuse reflectance spectra (DRS) of CdS NWs and CC NWs with different molar ratios of CuS (H). DRS of CdS NWs, CC-1 NWs and CCN NWs with different weight ratios of Ni_xP (I) (For interpretation of the references to colour in this figure legend, the reader is referred to the web version of this article.).

$g^{-1}\,h^{-1}$) than that of CCN NWs (**Fig. S3B**), elucidating the considerable contribution of CuS to the enhanced photoactivity over CCN NWs. Since Pt is always used as an efficient cocatalyst for photocatalytic H_2 evolution owing to its large work function [35], the H_2 evolution rate of CdS-Pt NWs with different weight ratios of Pt (**Fig. S3C**) and CC-Pt-1 has been tested. As shown in Fig. 3**A**, the H_2 evolution rate of optimal CdS-Pt-1 (3.16 mmol $g^{-1}\,h^{-1}$) and CC-Pt-1 (15.18 mmol $g^{-1}\,h^{-1}$) are both lower than that of CCN NWs, indicating that the well-designed CCN composite is an efficient noble-metal-free photocatalyst for H_2 evolution. The photocatalytic stability of the CdS NWs, CC NWs and CCN NWs for H_2 evolution has been evaluated by long-time experiments, which is as vital as photoactivity from the perspective of practical application. As shown in Fig. 3**B**, after 24 h of visible light irradiation, the H_2 production over CCN NWs is 30 times higher than that over blank CdS NWs. This result validates the markedly enhanced activity and good photostability of CCN NWs in current reaction conditions in comparison with bare CdS NWs. The morphology, crystal structures and optical properties of the fresh and used CCN NWs have been studied comparatively in **Fig. S4A-C**. These results evidence that no remarkable change of CCN NWs is found before and after long-time photoactivity test, further revealing the good stability of CCN NWs.

To decipher the cause of boosted activity of photocatalytic H_2 evolution of CCN NWs as compared with CdS and CC NWs, a series of photoluminescence (PL) and photoelectrochemical characterizations have been conducted to comparatively study the photogenerated electron-hole pairs separation and transfer process. Fig. 3**C** displays the polarization curves of bare CdS, CC and CCN NWs, from which it can be seen that the decoration of CuS onto CdS NWs leads to a slight increase of current density. The introduction of Ni_xP NPs obviously raises the current density, proving that Ni_xP NPs can act as an efficient cocatalyst for enhancing photocatalytic H_2 evolution due to the rapid electron transport and increased active sites [23]. The electrochemical impedance spectroscopy (EIS) has also been carried out to gain insight into the charge migration at the contacted interface between catalyst and electrolyte (Fig. 3**D**) [33]. The EIS plot of CCN NWs exhibits the smallest arc at high frequency among three catalysts, suggesting that a more efficient charge transfer and a smaller resistance between CCN NWs and electrolyte solution are acquired than those over CC NWs and CdS NWs [33]. The cyclic voltammograms (CV) in **Fig. S5A** show anodic and cathodic peaks of every catalyst. Since the preparation process of electrodes and electrolyte is alike for the measurements of CV curves, the current density of the electrodes is relevant to the electron transfer rate of the electrodes [36,37]. It is clearly seen that the current density over the electrodes of the CCN NWs is the biggest and that over the bare CdS NWs is the smallest, indicating that the introduction of CuS and Ni_xP can promote the electrons migrate across the contacted interface between electrode and electrolyte solution [38]. These results are further confirmed by the lifetime of photogenerated electrons,

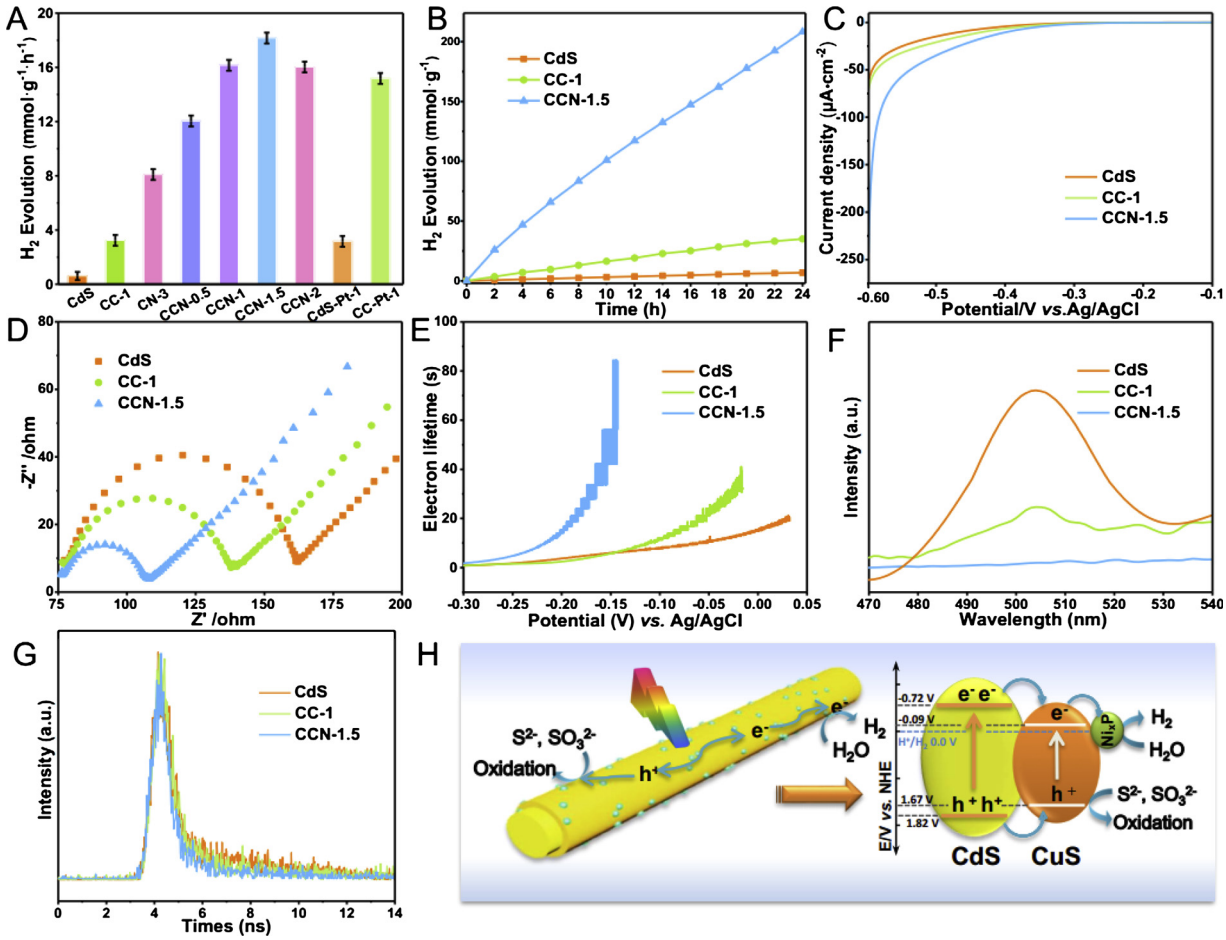

Fig. 3. Photocatalytic H_2 evolution over bare CdS, CC-1, CN-3, CCN NWs with different weight ratios of Ni_xP, CdS-Pt-1 and CC-Pt-1. Note that the error bars represent the photoactivity s.d. values calculated from triplicate experiments (A). Long-time experiments (B), polarization curves (C), EIS Nyquist plots (D), electron lifetime (E), steady-state photoluminescence (PL) emission spectra (F) with an excitation wavelength of 375 nm, time-resolved photoluminescence (TRPL) spectra decay (G) (excitation at 405 nm and emission at 520 nm) over CdS, CC-1 and CCN-1.5 NWs. Illustration of the proposed reaction mechanism for the photocatalytic H_2 production over CCN NWs under visible light illumination (H).

which has been measured by the open circuit photovoltage (V_{oc}) decay (OCP) technique under visible light irradiation. It can be seen from **Fig. S5B** and **3E** that the electron lifetime of CC NWs is much lower than that of CCN NWs and that of CdS NWs is the lowest. These results signify that the introduction of CuS and Ni_xP significantly decreases the recombination of photogenerated charge carriers and prolongs the lifetime of electrons. The PL spectra measured under 375 nm monochromatic light excitation have been used to gain more information of photoexcited electron-hole pairs. As depicted in Fig. 3**F**, the PL spectrum of CdS NWs exhibits an emission peak at around 500 nm, corresponding to the near-band-edge emission [2]. The PL intensity decreases after the decoration of CuS, while the PL signal is almost disappeared upon incorporating both CuS and Ni_xP NPs with CdS NWs. These experimental results clearly show that the recombination of photogenerated charge carriers in the CCN NWs is remarkably inhibited as compared with that of bare CdS NWs and CC NWs. Time-resolved photoluminescence (TRPL) spectra are used to study the specific charge carrier dynamics of the systems [39]. As shown in Fig. 3**G** and **Table S1**, the average emission lifetime, which reflects the overall emission decay behavior of the sample, displays an obvious decrease for CC NWs (4.66 ns) as compared with that of bare CdS NWs (7.27 ns). After depositing Ni_xP NPs onto the surface of CC NWs, the emission lifetime of the CCN NWs (3.95 ns) is further decreased. The observations of both PL quenching and emission lifetime reduction indicate the effect of CuS and Ni_xP for suppressing the recombination of photogenerated charge carriers. The above results together validate that the decoration of CuS and Ni_xP NPs onto the CdS matrix is able to synergistically boost the efficient separation and transfer of charge carriers, thereby accelerating the photocatalytic H_2 evolution rate.

It is evident that introducing Ni_xP NPs as a highly efficient cocatalyst is a prominent strategy for the enhanced H_2 evolution. This cocatalyst strategy can also be extended to other transition metal phosphide, such as Co_xP NPs that can be photodeposited onto the surface of CC core-shell NWs using the analogous preparation procedure. The TEM image shows that the Co_xP NPs with an average size of about 20 nm are anchored on the surface of CC NWs (**Fig. S6A**). The EDX spectroscopy (**Fig. S6C**) and XPS results (**Fig. S7A-F**) confirm the existence of Cd, S, Cu, Co and P elements in the CdS@CuS-Co_xP (CC-Co_xP) composite, further indicating that the CC-Co_xP NWs have been successfully prepared. As shown in **Fig S9**, similar to the role of Ni_xP NPs as a cocatalyst for assisting photocatalytic H_2 generation, the introduction of Co_xP NPs onto the surface of CC-1 NWs is also able to give rise to the obvious photoactivity enhancement of H_2 evolution. These results together validate the generality of transition metal phosphides as highly efficient cocatalysts for promoting photocatalytic H_2 evolution.

In terms of above analyses, the tentative mechanism for photocatalytic H_2 evolution over CCN NWs is proposed. As is clearly illustrated in Fig. 3**H**, CdS and CuS in CCN NWs are concurrently photoexcited under visible light illumination. On account of the suitable band alignment and close interfacial contact between CdS and CuS, the electrons can easily transfer to the conduction band (CB) of CuS from the CB of CdS, which follow the type-I charge transfer pathway [6].

Whereafter, the Ni_xP NPs anchored on the CdS@CuS NWs further capture and transfer the photogenerated electrons localized in the CB of CuS and act as proton reduction active sites to catalyze the surface reactions [23,40]. Simultaneously, the holes which transfer from valence band (VB) of CdS to the VB of CuS are trapped by sacrificial reagents. Taken together, such a well-designed three-level electron transfer pathway dramatically promotes the transfer of photogenerated charge carriers, thereby resulting in the boosted photocatalytic H_2 evolution over the ternary CCN NWs.

4. Conclusion

In summary, we have adopted CdS NWs as a 1D building block to construct a high-performance CdS@CuS-Ni_xP core-shell heterostructure catalyst *via* the combination of cation exchange and photoreduction deposition method. In this ternary composite, the matched energy level position and intimate interfacial contact between CdS and CuS lead to a type-I charge transfer pathway while Ni_xP NPs serve as cocatalyst to further capture the photogenerated electrons and provide active sites for proton reduction. Such a well-designed three-level electron transfer exerts a considerable influence on the separation and migration of photogenerated electron-hole pairs, thus contributing to the much higher photocatalytic activity of CCN NWs than that of bare CdS NWs and CC-Pt nanocomposite toward H_2 production. We anticipate that our work opens a new vista for constructing multicomponent 1D-based heterostructures with three-level charge transfer pathways for efficient solar-to-H_2 applications.

Declarations of interest

None.

Acknowledgements

The support from the National Natural Science Foundation of China (NSFC) (21872029, U1463204, 21173045), the 1st Program of Fujian Province for Top Creative Young Talents, the Award Program for Minjiang Scholar Professorship, the Independent Research Project of State Key Laboratory of Photocatalysis on Energy and Environment (NO. 2014A05), the Program for Returned High-Level Overseas Chinese Scholars of Fujian province and the Natural Science Foundation (NSF) of Fujian Province for Distinguished Young Investigator Rolling Grant (2017J07002) is gratefully acknowledged.

Appendix A. Supplementary data

Supplementary material related to this article can be found, in the online version, at doi:https://doi.org/10.1016/j.apcatb.2019.117934.

References

[1] L. Yuan, C. Han, M.-Q. Yang, Y.-J. Xu, Int. Rev. Phys. Chem. 35 (2016) 1–36.
[2] B. Han, S. Liu, N. Zhang, Y.-J. Xu, Z.-R. Tang, Appl. Catal. B 202 (2017) 298–304.
[3] Z. Sun, X. Liu, Q. Yue, H. Jia, P. Du, ChemCatChem 8 (2016) 157–162.
[4] Z.B. Yu, Y.P. Xie, G. Liu, G.Q. Lu, X.L. Ma, H.-M. Cheng, J. Mater. Chem. A 1 (2013) 2773–2776.
[5] L. Yuan, B. Weng, J.C. Colmenares, Y. Sun, Y.-J. Xu, Small 13 (2017) 1702253.
[6] M. Mahanthappa, N. Kottam, S. Yellappa, Appl. Surf. Sci. 475 (2019) 828–838.
[7] M.-Q. Yang, C. Han, Y.-J. Xu, J. Phys. Chem. C 119 (2015) 27234–27246.
[8] P. Jiang, Q. Liu, Y. Liang, J. Tian, A.M. Asiri, X. Sun, Angew. Chem. Int. Ed. 53 (2014) 12855–12859.
[9] H. Cheng, X.-J. Lv, S. Cao, Z.-Y. Zhao, Y. Chen, W.-F. Fu, Sci. Rep. 6 (2016) 19846.
[10] Q. Liu, J. Tian, W. Cui, P. Jiang, N. Cheng, A.M. Asiri, X. Sun, Angew. Chem. Int. Ed. 53 (2014) 6710–6714.
[11] H. Chen, Z. Sun, S. Ye, D. Lu, P. Du, J. Mater. Chem. A 3 (2015) 15729–15737.
[12] E.J. Popczun, J.R. McKone, C.G. Read, A.J. Biacchi, A.M. Wiltrout, N.S. Lewis, R.E. Schaak, J. Am. Chem. Soc. 135 (2013) 9267–9270.
[13] A. Indra, A. Acharjya, P.W. Menezes, C. Merschjann, D. Hollmann, M. Schwarze, M. Aktas, A. Friedrich, S. Lochbrunner, A. Thomas, M. Driess, Angew. Chem. Int. Ed. 56 (2017) 1653–1657.
[14] Z. Sun, Q. Yue, J. Li, J. Xu, H. Zheng, P. Du, J. Mater. Chem. A 3 (2015) 10243–10247.
[15] X.-T. Zhou, H.-B. Ji, X.-J. Huang, Molecules 17 (2012) 1149–1158.
[16] Z. Pu, Q. Liu, A.M. Asiri, X. Sun, ACS Appl. Mater. Interfaces 6 (2014) 21874–21879.
[17] D.P. Kumar, J. Choi, S. Hong, D.A. Reddy, S. Lee, T.K. Kim, ACS Sustainable Chem. Eng. 4 (2016) 7158–7166.
[18] Z. Qin, F. Xue, Y. Chen, S. Shen, L. Guo, Appl. Catal. B 217 (2017) 551–559.
[19] D. Zeng, W. Xu, W.-J. Ong, J. Xu, H. Ren, Y. Chen, H. Zheng, D.-L. Peng, Appl. Catal. B 221 (2018) 47–55.
[20] P. Ye, X. Liu, J. Iocozzia, Y. Yuan, L. Gu, G. Xu, Z. Lin, J. Mater. Chem. A 5 (2017) 8493–8498.
[21] S.-H. Li, N. Zhang, X. Xie, R. Luque, Y.-J. Xu, Angew. Chem. Int. Ed. 57 (2018) 13082–13085.
[22] P. Liu, J.A. Rodriguez, J. Am. Chem. Soc. 127 (2005) 14871–14878.
[23] T. Wu, P. Wang, J. Qian, Y. Ao, C. Wang, J. Hou, Dalton Trans. 46 (2017) 13793–13801.
[24] B. Weng, S. Liu, N. Zhang, Z.-R. Tang, Y.-J. Xu, J. Catal. 309 (2014) 146–155.
[25] S. Liu, M.-Q. Yang, Y.-J. Xu, J. Mater. Chem. A 2 (2014) 430–440.
[26] Y. Hong, J. Zhang, F. Huang, J. Zhang, X. Wang, Z. Wu, Z. Lin, J. Yu, J. Mater. Chem. A 3 (2015) 13913–13919.
[27] Y. Dong, L. Kong, P. Jiang, G. Wang, N. Zhao, H. Zhang, B. Tang, ACS Sustainable Chem. Eng. 5 (2017) 6845–6853.
[28] J. Zhang, J. Yu, Y. Zhang, Q. Li, J.R. Gong, Nano Lett. 11 (2011) 4774–4779.
[29] B.J. Beberwyck, Y. Surendranath, A.P. Alivisatos, J. Phys. Chem. C 117 (2013) 19759–19770.
[30] P.H.C. Camargo, Y.H. Lee, U. Jeong, Z. Zou, Y. Xia, Langmuir 23 (2007) 2985–2992.
[31] X. Zhan, Q. Wang, F. Wang, Y. Wang, Z. Wang, J. Cao, M. Safdar, J. He, ACS Appl. Mater. Interfaces 6 (2014) 2878–2883.
[32] J. Choi, D. Amaranatha Reddy, N.S. Han, S. Jeong, S. Hong, D. Praveen Kumar, J.K. Song, T.K. Kim, Catal. Sci. Technol. 7 (2017) 641–649.
[33] Y.-S. Xie, L. Yuan, N. Zhang, Y.-J. Xu, Appl. Catal. B 238 (2018) 19–26.
[34] Y. Chao, J. Lai, Y. Yang, P. Zhou, Y. Zhang, Z. Mu, S. Li, J. Zheng, Z. Zhu, Y. Tan, Catal. Sci. Technol. 8 (2018) 3372–3378.
[35] F. Wang, Y. Jiang, D.J. Lawes, G.E. Ball, C. Zhou, Z. Liu, R. Amal, ACS Catal. 5 (2015) 3924–3931.
[36] R. Wang, K.-Q. Lu, F. Zhang, Z.-R. Tang, Y.-J. Xu, Appl. Catal. B 233 (2018) 11–18.
[37] B. Weng, K.-Q. Lu, Z. Tang, H.M. Chen, Y.-J. Xu, Nat. Commun. 9 (2018) 1543.
[38] X. Xin, S.-H. Li, N. Zhang, Z.-R. Tang, Y.-J. Xu, Appl. Catal. B 245 (2019) 343–350.
[39] M.-Q. Yang, Y.-J. Xu, W. Lu, K. Zeng, H. Zhu, Q.-H. Xu, G.W. Ho, Nat. Commun. 8 (2017) 14224.
[40] J. Ran, J. Zhang, J. Yu, M. Jaroniec, S.Z. Qiao, Chem. Soc. Rev. 43 (2014) 7787–7812.